Iranian Journal of Geophysics, Vol 16 No 4, 2023, Page 175 – 192 (Research Article)
DOI:10.30499/IJG.2023.350587.1441

Evaluation of unstable points detection methods in geodetic GNSS-based networks

Zahra Banimostafavi[1], Mohammad Ali Sharifi[2*], Saeed Farzaneh[2]

[1]*M.Sc. Student of Geodesy, Department of Surveying and Geomatics Engineering, Faculty of Engineering, University of Tehran*
[2]*Associate Professor, Department of Surveying and Geomatics Engineering, Faculty of Engineering, University of Tehran*

(Received: 19 December 2019, Accepted: 9 March 2020)

Abstract

Deformation monitoring is a crucial engineering task for public safety. Any incorrect estimation of displacement rates can cause economical and deadly effects on engineering structures. Three methods have already been developed for structure deformation monitoring in the geodetic community: the single point method, and the robust and combinatorial estimation methods. In this article, the methods were implemented on a simulated dataset of the Global Navigation Satellite System. As a result, the Simultaneous Adjustment of Two Epochs and Multiple Sub Sample using distance differences methods were defined as the most optimal methods to find the stable and unstable points in the simulated network. To show the performance of the methods on a real dataset, the optimal methods were employed on the real GNSS observations collected of a pedestrian steel bridge in Tehran. The GNSS receiver type is LEICA GRX1200+GNSS. Moreover, two scenarios are investigated: all epochs have the same global coordinate systems (Scenario A), and analysis of the earth's surface movements with the local coordinate system in the first epoch of observations and the global WGS84 coordinate system for the others (Scenario B). The 3-D Helmert transformation was also used to transfer the global coordinate systems to the local one. Scenario B showed better results with a smaller RMS error with an amount of 7e-5.

Keywords: Deformation Monitoring, Single-point Analysis, Robust Estimation, Combinatorial Search Estimation, GNSS, SATE, MSS, M-split

[*]Corresponding author: sharifi@ut.ac.ir

1 Introduction

The Earth's layers move both horizontally and vertically due to many natural or artificial reasons such as changes in the groundwater level, tectonic activities, landslides, etc. These movements induce deformations and displacements in the manmade large engineering structures such as bridges, towers, and dams. For structural health monitoring, the structure response should be measured in a very careful way (Mohamed (2013)). There are two deformation monitoring techniques: geodetic and non-geodetic (geotechnical method) (Erol et al. (2004)). In non-geodetic techniques, the relative deformations are directly measured. The instruments like stress meters, inclinometers, piezometers, strain gauges, and extensometers are used in this technique (Dunnicli 1988, Teskey (1987)). In the geodetic monitoring methods, a geodetic network is designed in an optimal way. The network stations should repeatedly be observed in two or more epochs. The network observations analysis procedure includes three steps: Global Congruency Test to check the presence of displacement in each epoch, the unstable points rollout in each epoch or the so-called localization process, and finally estimation of displacement vectors. Two epochs under evaluation should have the same datum and network scale. Otherwise, the S-transformation will be used to unify the datum for both epochs.

This paper contains these sections: First, all deformation monitoring methods will be discussed in detail. Next, the presented methods will be examined on the simulated and real GNSS data, and the achieved results are evaluated. Finally, the paper ends up with a summary and conclusion.

2 Network analysis

The classical congruence analysis of geodetic networks consists of three major steps. After an adjustment of each epoch with the inner-constraint approach, first, the GCT is performed to examine the existence of deformations between epochs using the estimated results. Then, in the localization step, single-point, robust estimation, and combinatorial search methods will be applied on two epochs under comparison with the same datum in the network. On the other hand, because of many environmental reasons such as different atmospheric conditions in each observation campaign, an S-transformation is used to transfer the datum of each epoch to a common one. Furthermore, using different uncalibrated instruments for collecting measurements in successive epochs may cause problems. This can change network scale between epochs and cause multiple errors in deformation analysis. Thus, the scale-independent determination of deformations, combination of different data types, different setups of the coordinate system, and the choice of instrumentation, are the reasons for development of the new methods of analysis (Ebeling (2014)).

3 Deformation analysis

To detect any probable displacement in engineering structures, we need a geodetic monitoring network (Welsch, Heunecke et al. (2000)). It can be detected using well-mounted benchmarks at specific places on the structure. At first, the estimated variance test is used for compatibility comparison of the results from different epochs. This test is done by the estimated variance of epoch *i* and epoch *j* as follows:

Null hypothesis H_0:

$$E\{\hat{\sigma}_{0_i}^2\} = E\{\hat{\sigma}_{0_j}^2\} \quad (1)$$

Alternative hypothesis H_A:

$$E\{\hat{\sigma}_{0_i}^2\} \neq E\{\hat{\sigma}_{0_j}^2\} \quad (2)$$

Test statistic:

$$T_F = \frac{\hat{\sigma}_{0_i}^2}{\hat{\sigma}_{0_j}^2} \quad (3)$$

If the test statistic cT_F fits with Fisher-distribution, that means the null

hypothesis H_0 cannot be refused. Then, the deformation analysis procedure can be started.

$$T_F \leq F_{s=1-\alpha/2, f_1=r_i, f_2=r_j} \quad (4)$$

Where α is the defined significance level for the test, r_j and r_j are the network redundancies for epochs *i* and *j* (Welsch, Heunecke et al. (2000)). Further information can be found in (Grundig (1985); Gründig, Neureither et al. (1985)).

3.1 GCT

To start the deformation monitoring procedure, first, the GCT should be run on the estimated results of two epochs. If this test passes the results are comparable. (Amiri-Simkooei, Alaei-Tabatabaei et al. (2016)). If the H_0 hypothesis is true, there isn't any deformation between epoch *i* and *j*. Where $\vec{x}_i$ and $\vec{x}_j$ are the adjusted coordinate of epoch *i* and *j*.

$$\vec{x}_i - \vec{x}_j = \vec{0} \quad (5)$$

If the test in (4) passes, the combined variance factor $\hat{\sigma}_0^2$, for both epochs equal to

$$\hat{\sigma}_0^2 = \frac{\vec{v}_i^T P_i \vec{v}_i + \vec{v}_j^T P_j \vec{v}_j}{r_i + r_j} = \frac{r_i \hat{\sigma}_{0_i}^2 + r_j \hat{\sigma}_{0_j}^2}{r_i + r_j} \quad (6)$$

where P_i and P_j are the weight matrices, $\vec{v}_i$ and $\vec{v}_j$ are the estimated residual vectors, r_i and r_j are the network redundancies for epochs *i* and *j*. If the $\vec{d}$ is the deformation between two epochs:

$$\vec{d} = \vec{x}_i - \vec{x}_j \quad (7)$$

According to covariance propagation law, the corresponding weight matrix P_{dd} can be calculated by $Q_{xx_i}$and Q_{xx_j}which are the cofactor matrices of epoch *i* and *j*.

$$P_{dd} = (Q_{xx_i} + Q_{xx_j})^{-1} \quad (8)$$

If we assume the observations are independently measured in two epochs, the quadratic form $\hat{\Omega}^2$ can directly be calculated from the results of the individual adjustments of each epoch.

$$\hat{\Omega}^2 = \frac{\vec{d}^T P_{dd} \vec{d}}{h} \quad (9)$$

where h is equal to b - d, where b is the total number of the condition equations and d is the rank defect of the weight matrix P_{dd}. These can be determined using:

$$dl = l_i - l_j = A_i^T \vec{x}_i - A_j^T \vec{x}_j \quad (10)$$

l_i and l_j are observation vectors, $dl$is the observation difference, A_i and A_j are design matrices of epoch *i* and *j*. Their cofactor matrix follows:

$$Q_{dl} = A_i^T Q_{xx_i} A_i + A_j^T Q_{xx_j} A_j$$
$$h = rk(Q_{dl}) = rk(P_{dd}) \quad (11)$$

Then, the quadratic form $\hat{\Omega}^2$ can directly be calculated using the estimated results of the epochs:

$$\hat{\Omega}^2 = \frac{d\vec{l}^T Q_{dl}^{-1} dl}{\hat{\sigma}_0^2 h} \quad (12)$$

As seen, the two quantities $\hat{\Omega}^2$ and $\hat{\sigma}_0^2$ are stochastically independent and can therefore be contrasted using the global congruency test as below.

Null hypothesis H_0:

$$E\{\hat{\sigma}_0^2\} = E\{\hat{\Omega}^2\} \quad (13)$$

Alternative hypothesis H_A:

$$E\{\hat{\sigma}_0^2\} < E\{\hat{\Omega}^2\} \quad (14)$$

Statistical Test:

$$T_G = \frac{\hat{\Omega}^2}{\hat{\sigma}_0^2} \quad (15)$$

If the result of T_F agrees with Fisher-distribution, that means:

$$T_G \leq F_{s=1-\alpha/2, f_1=h_i, f_2=r_i+r_j} \quad (16)$$

With a given significance level α and the degrees of freedom $f_1 = h$ and $f_2 = r_i + r_j$ (the sum of the network redundancies), $\hat{\sigma}_0^2$ and $\hat{\Omega}^2$ must be considered statistically identical. Alternatively, if the global congruency test fails, the existence of deformations between the two epochs is expected (Ebeling (2014)).

3.1.1 Single point analysis

This is the simplest and most common method in deformation analysis. The achieved results are influenced by the classic congruence method in the stability

identification of every single point in a geodetic network.

- **Simultaneous Analysis of Two Epochs (SATE)**

In the classical approaches, the least-squares estimation is applied on the collected observations of each epoch. However, the methods will encounter many problems when a large set of different observation-type is simultaneously processed. The SATE scheme is a new method developed based on the Baarda theory (Baarda (1968); Teunissen (2000), and Teunissen et al. (2005) , Amiri-Simkooei and Asgari (2012), Amiri-Simkooei, Tiberius et al. (2007), and Amiri-Simkooei, Zaminpardaz et al. (2014)). To detect stable/ unstable points, the method is based on two hypotheses on the functional model. In the null hypothesis, all points of the geodetic network are assumed to be stable between two epochs. However, In the alternative hypothesis, it is assumed at least one point is subject to displacement (Amiri-Simkooei, Alaei-Tabatabaei et al. (2016)).

Model 1:

$$\begin{cases} H_0: E\{\hat{d}\} = 0 \\ E\{\vec{l}\} = A\vec{x} \end{cases} \quad (17)$$

Null hypothesis H_0:

$$H_0: E(\vec{l}) \sim N_m(Ax, C_y) \quad (18)$$

Model 2:

$$\begin{cases} H_a: E\{\hat{d}\} \neq 0 \\ E\{\vec{l}\} = [A, B]\begin{bmatrix} \vec{x} \\ \zeta \end{bmatrix} = A\vec{x} + B\zeta \end{cases} \quad (19)$$

Alternative hypothesis H_A:

$$H_a: E(\vec{l}) \sim N_m(Ax + B\zeta, C_y) \quad (20)$$

In Eq. (17), $m \times 1$ vector $\vec{l}$ and $\vec{x}$ $n \times 1$ vector are the observations and the unknown parameters vectors, respectively. A is design matrix, ζ is the displacement of the unstable points between two epochs with an appropriate design matrix represented by B. N_m is an m-dimensional normal distribution with $C_y$covariance matrix of the observations. In both models, all stochastic characters of the observations are considered to be the same. The so-called σ is assumed to be known. Hence, the statistical test is defined as:

$$T_q = \hat{e}_0^T C_y^{-1} \hat{e}_0 - \hat{e}_a^T C_y^{-1} \hat{e}_a \quad (21)$$

where $\hat{e}_0$ and $\hat{e}_a$ are the least squares estimated residuals and q is the additional unknowns in the alternative hypothesis. The chi-square distribution is a criteria for the above test criterion. (Teunissen, Simons et al. (2005), Amiri-Simkooei (2016)).

$$H_0: T_q \sim \chi^2(q, 0), H_a: T_q \sim \chi^2(q, \lambda) \quad (22)$$

Where the non-centrally parameter λ and $P_A^{\perp}$the orthogonal projector are:

$$P_A^{\perp} = I_m - A(A^T C_y^{-1} A)^{-1} A^T C_y^{-1} \quad (23)$$

$$\lambda = \zeta^T B P_A^{\perp} C_y^{-1} B\zeta = \|P_A^{\perp} B\zeta\|_{C_y^{-1}} \quad (24)$$

the variance factor of the unit weight calculates, $C_y = \sigma_0^2 Q$, where Q is the known cofactor matrix (Amiri-Simkooei et al. (2016)):

$$T_q = \frac{1}{q\hat{\sigma}_a^2} \hat{\zeta}^T B^T Q^{-1} Q_{\hat{e}_0} Q^{-1} B\hat{\zeta} \quad (25)$$

Assuming the alternative hypothesis, $\hat{\sigma}_a^2$ is an unbiased estimate of the variance factor and $Q_{\hat{e}_0}$is the cofactor matrix of the least-squares residuals under the null hypothesis.

$$\hat{\sigma}_a^2 = \frac{\hat{e}_a^T Q^{-1} e_a}{m - n - q} \quad (26)$$

The statistical distribution of the given test is (Teunissen, Simons et al. (2005)):

$$\begin{aligned} H_0: T_q &\sim F(m - n - q, 0) \\ H_a: T_q &\sim F(m - n - q, \lambda) \end{aligned} \quad (27)$$

where the m and n are the dimensions of the observations and unknown vectors. The non-centrally parameter λ is given as (Amiri-Simkooei, Alaei-Tabatabaei et al. (2016)):

$$\lambda = \frac{1}{\sigma^2} \zeta^T B^T Q^{-1} Q_{\hat{e}_0} Q^{-1} B\zeta \quad (28)$$

In this procedure, we first determine the coordinates of the points in each epoch using the inner-constraint method. Fisher's distribution is then used to determine T_q using the initial values. The most unstable point corresponds to the highest T_q value. The unstable point is eliminated and the new test value is calculated in the absence of the most unstable point. The new value and Fisher's distribution are compared. The second point with the highest T_q value is eliminated if the alternative test (Eq. 20) is rejected. The procedure is continued until all unstable points are found.

The problem with the single-point analysis method is that the method doesn't give the best results if a large number of points have displacement or any additional systematic error occurs between the epochs. Besides, this method checks each point of the network separately while the others assumed to be fixed. It increases the false detection of stable/ unstable points. Moreover, this method is based on the least squares estimation with the prerequisite of systematic error-free observations contaminated with the Gaussian noise. Otherwise, it leads to a wrong solution.

3.1.2. Combinatorial Search

The two above methods, the classical Least-Squares-based single point analysis or the robust estimation techniques cannot yield reliable results in all casesdue their dependence on the network geometry (Ebeling (2014)). The new method, defined by Nietzel (2004) the so-called *Maximum Sub Sample* (MSS) method, and the M-split method substituted it, are the combinatorial search methods.

- **The Multiple Sub Sample using distance differences**

In this method, all possible distances between points in the network are computed from the adjusted coordinates in both epochs of *i* and *j*. According to the covariance law, their corresponding cofactor matrix is derived as (Ebeling (2014)):

$$l_i = A_i^T \vec{x}_i, Q_{ll_i} = A_i^T Q_{xx_i} A_i \quad (29)$$

$$l_j = A_j^T \vec{x}_j, Q_{ll_j} = A_j^T Q_{xx_j} A_j \quad (30)$$

First, with inner constraint estimates of the unknowns are calculated. Where l_i and l_j are the observations vectors, A_i and A_j are the design matrices, $Q_{xx_i}$and $Q_{xx_j}$are the covariance matrices of the unknowns in the epoch *i* and *j*. Then the distance difference observation matrix dl and its cofactor matrix Q_{dl} follows:

$$dl = l_i - l_j \qquad Q_{dl} = Q_{ll_i} + Q_{ll_j} \quad (31)$$

With the combined variance factor of both epochs $\hat{\sigma}_0^2$, the standard deviation $\hat{\sigma}_{dl}$ for the distance differences is available. With these observations, we can identify which distances have significant changes between the epochs. Each distance observation rejected in this test is subject to an observation blunder (Ebeling (2014)).

$$|dl_k| > T\hat{\sigma}_{dl_k} \quad (32)$$

where *T* is an experimental value (between 3 and 5). Considering a very high value leads to acceptance of most observations while with a low value most observations are rejected. Each rejected observation in this test will be deleted. In the second step, the unknowns are calculated using the remaining observations via the least squares estimation (Ebwateling (2014)).

- **The Multiple Sub Sample using angles**

For a network with direction-only observations the scale factors cannot be computed. Only approximate error estimates are available and hard thresholds for distance ratios cannot be determined. The least squares fit must then be computed for each candidate point to estimate the unknown scale factor and identify the correct solution. This makes the MSS distance ratio computationally

more expensive than the distance difference approach. The range ratio MSS is not used in this article due to its density and time-consuming computational process. In contrast, using the angle between epochs reduces computation time. This method excludes and examines angles that exhibit large changes. The number of angle observations for an epoch is less than the number of distances measurements. The distance difference approach is not applicable when the scale changes between the epochs. The angle-based MSS approach combines the advantages of both distance-based MSS methods. Another advantage of the MSS method in general is the location of the largest similar point group. These points can be performed independently of the coordinate system and date definition of the respective epoch, as only date-invariant elements (lengths and angles) are used Ebeling (2014).

- **M-split**

Finding stable points in a geodetic control network affected by datum defect problems is difficult. A considerable number of data can aggravate this problem. (CHEN (1983), Baselga, García-Asenjo et al. (2015), Amiri-Simkooei et al. (2016), and Aydin (2017)).

Wiśniewski (2009, 2010) introduces the M-split method based on a robust M-estimation (Wiśniewski (2009), Wiśniewski (2010)). Figure 1 shows the differences between the results of the robust M-estimation, the Msplit (q) estimation, and the least squares estimation on a given sample (Nowel (2018)). The M-split is a new method, that is based on a simultaneous and joint optimization process. (Nowel (2018) and Wiśniewski (2008, 2009)).

If we assume the two-dimensional problem, this consists of (q=2) local congruence models, therefore each value of the raw displacement vector can be a priori realization of each model (Nowel (2018)).

$$W_k^1 = diag((\hat{d}_{1(2)}^{k-1})^2 ....(\hat{d}_{u(2)}^{k-1})^2) \quad (33)$$

$$\hat{d}_1^k = (I - H(H^T W_{(1)}^k H)^{-1} H^T W_{(1)}^k)\Delta\hat{x}$$

$$W_k^2 = diag((\hat{d}_{1(1)}^{k})^2 ....(d_{u(1)}^{k})^2) \quad (34)$$

$$d_2^k = (I - H(H^T W_{(2)}^k H)^{-1} H^T W_{(2)}^k)\Delta\hat{y}$$

Where $\hat{d}_1$ and $\hat{d}_2$ are the displacement component for x and y, W^1 and W^2 are the calculated weight from displacement vectors for x and y, and H is a datum matrix. If $Q_{\hat{d}}$ is the cofactor matrix of estimated displacement vector of all points.

$$Q_{\hat{d}}^{+} = (Q_{\hat{d}} + HH^T)^{-1} Q_{\hat{d}} (Q_{\hat{d}} + HH^T)^{-1} \quad (35)$$

The global and local F-test is:

$$T = \frac{\hat{d}^T Q_{\hat{d}}^{+} \hat{d}}{r\sigma_0^2} < F(r, df) \quad (36)$$

Where $r = rank(Q_{\hat{d}})$, the variance factor estimator $\hat{\sigma}_0^2 = \frac{\hat{\sigma}_{0_1}^2 + \hat{\sigma}_{0_2}^2}{2}$, and $df = df_1 + df_2$ is the network of freedom. The criterion of the test is Fisher-distribution. The test rejection shows possible displacement. The test should repeat for all points (Nowel (2018)).

$$T_{i(j)} = \frac{\hat{d}_{i(j)}{}^T Q_{\hat{d}_{i(j)}}^{-1} \hat{d}_{i(j)}}{r_i \sigma_0^2} < F(r_i, df) \quad (37)$$

Where $r_i = rank(Q_{\hat{d}_i})$, and $Q_{\hat{d}_{i_{(j)}}}$ is the cofactor matrix of estimated displacement vector of point i for model j (Caspary (2000) and Nowel (2016, 2018)).

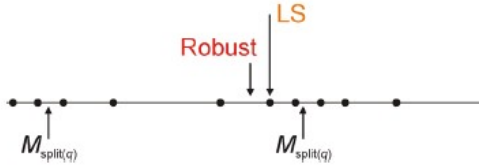

Figure 1. Comparison of the M-split (q) with q =3, robust M-estimation, and LS estimation (Wiśniewski (2009, 2010), and Nowel (2018))

4 The Helmert-transformation

If two epochs under comparison have different coordinate systems, the Helmert

transformations should be operated on estimated coordinates. We have seven parameters in a 3-D network to define the geodetic datum completely: three rotations parameters defining the orientation of the coordinate axes $(\omega, \varphi, \kappa)$, three translations defining the origin (T_x, T_y, T_z), and a scale factor (λ) defining distances in the coordinate system. It can be written as (Ebeling (2014)):

$$\vec{x}_i = \lambda . R . \vec{x}_j + \vec{T} \tag{38}$$

$$\begin{bmatrix} x \\ y \\ z \end{bmatrix}_i = \lambda R_z(\kappa) R_y(\varphi) R_x(\omega) \begin{bmatrix} x \\ y \\ z \end{bmatrix}_j + \begin{bmatrix} T_x \\ T_y \\ T_z \end{bmatrix} \tag{39}$$

To solve the equations, at least three points with known coordinates in both systems (local and global) are needed to find the unknown transformation parameters. If the coordinates $\vec{x}_i$ and $\vec{x}_j$ are obtained in a free network adjustment, their corresponding cofactor matrices Q_{xx_i}, and Q_{xx_j} are singular (Ebeling (2014)).

5 Results

Herein, we use both simulated and real GNSS observations to show performance of the introduced methods. The results, their initial analysis, and the priority reasons for each method are explained. İn order to detect stable/unstable points, three methods are employed: the single-point analysis, the robust estimation techniques, and the combinatorial search method. The methods are implemented on the simulated data and the most successful method is implemented on the real data.

5.1.1 GNSS simulated data

A network of nine points is used to evaluate the performance of the proposed methods. Points 5-9 are shifted in the second epoch to show a significant shift between the two epochs. Tables 2-4 present the amounts of shifts. By applying different displacement values, in three cases, the success rate of different methods in detecting unstable points are compared. The results were evaluated at a significance level of 0.99. The success of different methods in this data is compared with each other. The 3D coordinates of the monitoring points are in a WGS84 global coordinate system. The true coordinates of the first epoch are listed in Table 1.

Table 1. The first epoch coordinates of GNSS observations

Point number	X (m)	Y (m)	Z (m)
1	3225238.342	4052706.572	3712624.904
2	3238443.659	4060239.722	3691798.557
3	3247605.217	4038624.398	3707994.103
4	3245085.094	4050269.748	3697002.558
5	3221372.091	4062200.733	3705189.488
6	3240499.215	4049740.067	3701662.681
7	3234236.838	4053154.284	3703562.939
8	3234478.242	4053333.42	3703078.49
9	3234261.284	4053129.146	3703552.643

A horizontal plot of the network points is shown in Fig. 2. The simulated coordinates for the subsequent epochs are obtained by adding simulated deformations for each epoch to the coordinates of the base epoch.

- **Baseline Processing**

As we know, processing the baselines is an essential and primary job for static positioning Curran (2008). Four stations of the network (points 1-4) were chosen as fixed points. The observations consist of horizontal distances. We added a gaussian random noise to observations with standard deviations of about $\pm(4\text{mm} + 5\text{ppm})$ for horizontal distances.

Three cases are considered for displacement in stations 5-9. The assumed

displacement values over the points are listed in Tables 2-4.

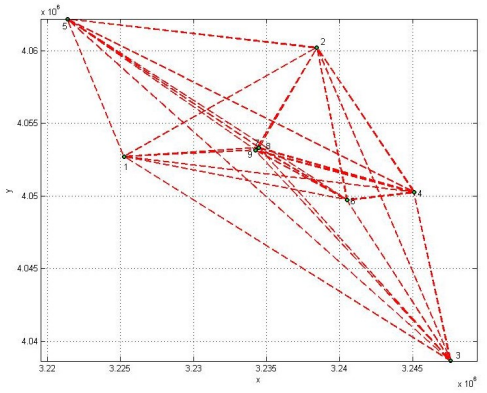

Figure 2. The simulated data network

Table 2. Real deformation of the points for case 1 in meters

	First case			
Point	ΔX	ΔY	ΔZ	Norm
5	0.337	0.166	0.748	0.837
6	0.162	0.602	0.450	0.769
7	0.794	0.263	0.083	0.841
8	0.311	0.654	0.229	0.76
9	0.529	0.689	0.913	1.26

Table 3. Real deformation of the points for case 2 in meters

	Second case			
Point	ΔX	ΔY	ΔZ	Norm
5	0.015	0.044	0.082	0.094
6	0.083	0.01	0.087	0.120
7	0.054	0.097	0.008	0.111
8	0.10	0.001	0.04	0.107
9	0.008	0.077	0.026	0.082

Table 4. Real deformation of the points for case 3 in meters

	Third case			
Point	ΔX	ΔY	ΔZ	Norm
5	0.008	0.001	0.001	0.008
6	0.004	0.001	0.009	0.01
7	0.009	0.009	0.006	0.014
8	0.002	0.006	0.004	0.007
9	0.002	0.005	0.005	0.008

- **Results of network analyses**

The inner-constraint approach was run to find the adjusted coordinates, and the results were accepted at the significance level of 0.99 in the estimated factor variance test. The success of single point analysis, robust estimation, and combinatorial search methods are compared. In each epoch, 108 observations were collected. The parameter vector consists of 27 unknowns and 3 datum defects. The achieved results are given in table 5.

Table 5. The GCT test to confirm the displacement between two epochs

T_G (First case)	T_G (Second case)	T_G (Third case)	Fisher (α=0.025, β=20)	Situation
115.4	129.5	59.73	1.76	There is the displacement between two epochs

- **Localization**

In the first step, point 5 is displaced, and calculated the success rate of each method. Then, points 5 and 6 are displaced. In every step, one point is added until at last 5 points are displaced. The success rate and the unstable points for different cases are presented in diagrams Figs. 3-5:

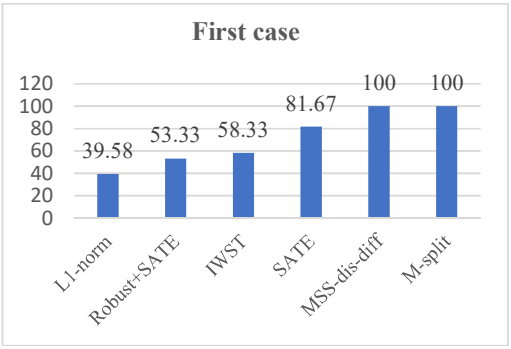

Figure 3. The success rate of different methods of the simulated GNSS data (Case #1)

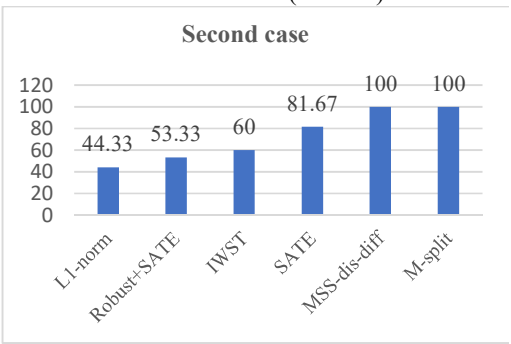

Figure 4. The success rate of different methods of the simulated GNSS data (Case #2).

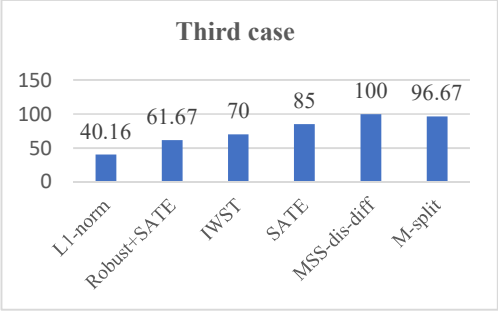

Figure 5. The success rate of different methods of the simulated GNSS data (Case #3)

- **Determination of point deformation**

After the identification of all unstable and stable points, the final task is now to determine the deformations and their standard deviations. The network analysis is repeated. The stable points are now considered fixed points, and the estimated deformation is presented in Tables 6-8. A Summary of the cases and methods is given in Table 9.

Table 6. Estimated displacement of the simulated GNSS observations in meters (Case #1)

	First case			
Point	ΔX	ΔY	ΔZ	Norm
5	0.337	0.166	0.748	0.837
6	0.162	0.602	0.450	0.769
7	0.794	0.263	0.083	0.841
8	0.311	0.654	0.229	0.76
9	0.529	0.689	0.913	1.26

Table 7. Estimated displacement of the simulated GNSS observations in meters (Case #2)

	Second case			
Point	ΔX	ΔY	ΔZ	Norm
5	0.015	0.044	0.082	0.094
6	0.083	0.01	0.087	0.120
7	0.054	0.097	0.008	0.111
8	0.1	0.001	0.04	0.107
9	0.008	0.077	0.026	0.082

Table 8. Estimated displacement of the simulated GNSS observations in meters (Case #3)

	Third case			
Point	ΔX	ΔY	ΔZ	Norm
5	0.008	0.001	0.001	0.008
6	0.004	0.001	0.009	0.01
7	0.009	0.009	0.006	0.014
8	0.002	0.006	0.004	0.007
9	0.002	0.005	0.005	0.008

Table 9. Summary of statistics for combined readjustment of epochs

	Case #1	Case #2	Case #3
Number of points in the network	9	9	9
Number of observations	216	216	216
Number of unknowns	27	27	27
Redundancy	84	84	84
A posteriori standard deviation $\hat{\sigma}_0$	0.033	0.038	0.022
Lower boundary value $\chi^2_{S=0.025,r}$ in second-factor variance test	56.813	56.813	56.813
T_F in second-factor variance test	91.465	68.476	59.73
Upper boundary value $\chi^2_{S=0.975,r}$ in second-factor variance test	117.057	117.057	117.057
The outcome of the second-factor variance test	pass	pass	pass

Finally, the comparison of true and estimated deformations and displacements should be compared to evaluate the accuracy of the deformation monitoring. The difference between the true and calculated displacement of simulated GNSS observations is tabulated in Table 10-12.

Table 10. Difference between the true and calculated displacement in the simulated GNSS observations in meters (Case #1)

Point	e_x	e_y	e_z
5	0.212	0.244	0.216
6	-0.339	-0.432	-0.384
7	0.342	0.401	0.333
8	1.54	3.254	-5.516
9	0.283	0.352	0.336

Table 11. Difference between the true and calculated displacement in the simulated GNSS observations in meters (Case #2)

Point	e_x	e_y	e_z
5	0.789	0.967	0.853
6	-0.309	-0.403	-0.357
7	0.085	0.081	0.061
8	1.433	4.258	-5.818
9	7.31	3.331	-1.436

Table 12. Difference between the true and calculated displacement in the simulated GNSS observations in meters (Case #3)

Point	e_x	e_y	e_z
5	0.789	0.967	0.853
6	-0.309	-0.403	-0.356
7	0.085	0.0813	0.061
8	1.433	4.258	-5.818
9	7.31	3.331	-1.436

The SATE is selected as the optimal method among single-point analysis methods due to the simultaneous adjustment of two epochs and use of two groups of observations and can detect the unstable points with the highest rate of accuracy. In the combinatorial method, an MSS using distance differences always could detect unstable points and be selected as the optimal method. The results of displacement calculation are very close to the original simulated values. Thus, by ensuring the results in the simulated data, we apply optimal methods to evaluate real GNSS data of some areas in Tehran. The type of GPS receiver is LEICA GRX1200+GNSS.

5.1.2 Implement the optimal method using real GNSS data

These observations include nine stations in Tehran, that have been measured in four epochs. The points with the WGS84 cartesian coordinate system are shown in the following tables. For this purpose, the optimally selected methodologies should be operated on real data. The coordinates of these epochs are:

Table 13. Stations WGS84 cartesian coordinates of the first
The epoch of the real GNSS observations

# Point	X (m)	Y (m)	Z (m)
DA01 (1)	3225238.342	4052706.572	3712624.904
M020 (2)	3238443.659	4060239.722	3691798.557
M022 (3)	3247605.217	4038624.398	3707994.103
M318 (4)	3245085.094	4050269.748	3697002.558
M804 (5)	3221372.091	4062200.733	3705189.488
THEN (6)	3240499.215	4049740.067	3701662.681
TMIC (7)	3234236.838	4053154.284	3703562.939
M_10 (8)	3234478.242	4053333.42	3703078.49
M_20 (9)	3234261.284	4053129.146	3703552.643

Table 14. Stations WGS84 cartesian coordinates of the second
The epoch of the real GNSS observations

# Point	X (m)	Y (m)	Z (m)
DA01 (1)	3225238.342	4052706.572	3712624.904
M020 (2)	3238443.659	4060239.722	3691798.557
M022 (3)	3247605.217	4038624.398	3707994.103
M318 (4)	3245085.094	4050269.748	3697002.558
M804 (5)	3221372.091	4062200.733	3705189.488
THEN (6)	3240499.215	4049740.067	3701662.681
TMIC (7)	3234236.838	4053154.284	3703562.939
M_10 (8)	3234478.396	4053333.745	3703077.939
M_20 (9)	3234261.284	4053129.146	3703552.643

Table 15. Stations WGS84 cartesian coordinates of the third
The epoch of the real GNSS observations

# Point	X (m)	Y (m)	Z (m)
DA01 (1)	3225238.342	4052706.572	3712624.904
M020 (2)	3238443.659	4060239.722	3691798.557
M022 (3)	3247605.217	4038624.398	3707994.103
M318 (4)	3245085.094	4050269.748	3697002.558
M804 (5)	3221372.091	4062200.733	3705189.488
THEN (6)	3240499.215	4049740.067	3701662.681
TMIC (7)	3234236.838	4053154.284	3703562.939
M_10 (8)	3234478.413	4053333.372	3703077.953
M_20 (9)	3234261.277	4053129.209	3703553.131

Table 16. Stations WGS84 cartesian coordinates of the fourth
The epoch of the real GNSS observations

# Point	X (m)	Y (m)	Z (m)
DA01 (1)	3225238.342	4052706.572	3712624.904
M020 (2)	3238443.659	4060239.722	3691798.557
M022 (3)	3247605.217	4038624.398	3707994.103
M318 (4)	3245085.094	4050269.748	3697002.558
M804 (5)	3221372.091	4062200.733	3705189.488
THEN (6)	3240499.215	4049740.067	3701662.681
TMIC (7)	3234236.838	4053154.284	3703562.939
M_10 (8)	3234478.385	4053333.846	3703077.909
M_20 (9)	3234261.357	4053129.479	3703552.499

The network with nine stations distributed over the city Tehran and the Google Earth image as the background is illustrated in Fig. 6.

Figure 6. The network of points in google earth

1. Scenario A

In Scenario A, all epochs have the same coordinate system and refer to the same computational base with no scale change (Ebeling (2014)).

- **Results of network analyses**

First, the observations were evaluated by the Inner-constraint approach and accepted in the second-factor variance test in 0.99. Second, a GCT test is performed on the displacement vector of the two-time epochs to check for the presence of displacements between the epochs in the first case.

- **Localization**

With the outcome of the GCT in mind, the next step is now to identify stable and unstable points. This is done with SATE and MSS using distance difference methods. The detected stable and unstable points of each method are presented in Table (18).

- **Determination of point deformation**

After detection of all unstable and stable points, the final task is now to calculate the deformations and their standard deviations. The network analysis is repeated, and the stable points are now considered known calculated points. The calculated deformation is presented in Tables (19-21). A Summary of the cases and methods is given in Table (22).

Table 17. The GCT test to confirm the displacement between two epochs

T_G (Epoch 1-2)	T_G (Epoch 1-3)	T_G (Epoch 1-4)	$F_{\alpha,\beta}$ (α=0.025, β=80)	Comment
86.96	63.51	46.24	1.616	There is possible displacement between two epochs

Table 18. Stable/unstable points using the chosen methods (α=0.025 and β=20) the Fisher-distribution

	Epoch 1-2		Epoch 1-3		Epoch 1-4	
Method	MSS using distance difference	SATE	MSS using distance difference	SATE	MSS using distance difference	SATE
Stable	1,2,3,4,5,6,7,9	1,2,3,4,5,6,7,9	1,2,3,4,5,6,7	1,2,3,4,5,6,7	1,2,3,4,5,6,7	1,2,3,4,5,6,7
Unstable	8	8	8,9	8,9	8,9	8,9

Table 19. Estimated deformations of network points in scenario A in meters

Epoch 1-2					
# Point	ΔX	ΔY	ΔZ	Norm	Direction (rad)
8	0.154	0.325	-0.552	0.659	1.128

Table 20. Estimated deformations of network points in scenario A in meters

Epoch 1-3					
# Point	ΔX	ΔY	ΔZ	Norm	Direction (rad)
8	0.171	-0.048	-0.537	0.566	-0.273
9	-0.007	0.063	0.488	0.492	1.676

Table 21. Estimated deformations of network points in scenario A in meters

Epoch 1-4					
# Point	ΔX	ΔY	ΔZ	Norm	Direction (rad)
8	0.143	0.426	-0.582	0.735	1.246
9	0.073	0.333	-0.144	0.370	1.355

Table 22. Summary and statistics for the combined re-adjustment of the epochs

	1st epoch	2nd epoch
Number of points in the network	9	9
Number of observations	87	87
Number of unknowns	27	27
Redundancy	63	63
A posteriori standard deviation $\hat{\sigma}_0$	0.58	0.76
Lower boundary value $\chi^2_{S=0.025,r}$ in second-factor variance test	39.86	39.86
T_F in second-factor variance test	50.16	77.25
Upper boundary value $\chi^2_{S=0.975,r}$ in second-factor variance test	92.01	92.01
The outcome of the second-factor variance test	Pass	pass
RMSE	6.98e-06	6.96e-06

2. Scenario B

The movement of Earth's crust causes no certain stable point in observations. Every point on the Earth, including the stable points, move from time to time. We suppose to use the local coordinate system for the base epoch, and the global coordinate system chosen for the other epochs. In this regard, the 3-D Helmert transformation should be used (Ebeling (2014)). As we know, the coordinates of GPS measurements are the WGS84 Cartesian coordinate system. To see the real directions of the displacements, all WGS-84 Cartesian should transform to a local topocentric coordinate system because the obtained directions in this system are incompatible with directions on the physical ground. Thus, cartesian coordinates in the WGS-84 coordinate system must transform the plane coordinate system. For this process, we need at least three points of known coordinates in the national coordinate system. This process requires more time and additional processes. As a substitution, cartesian coordinates in the WGS84 system are transformed to the local topocentric coordinate system with the T transformation equation (Taşçi (2008)), but this process is not included in this research, and 3-D Helmert transformation is used as the substitution, because in this transformation the rotation, translation, and scale factor can be calculated. The calculated coordinates that define the reference

frame for epochs 2-4 are listed in the tables below, and in the local system of epoch 1, the same approximate coordinates as for the previous scenario are used, which are shown in Tables (23-25). The transformation parameters relating to the global and the local systems are given in Table (26)

Table 23. Stations WGS84 cartesian coordinates of the second epoch of the real GNSS observations

# Point	X (m)	Y (m)	Z (m)
DA01 (1)	6460932.675	8105310.413	7415569.323
M020 (2)	6474138.006	8112843.571	7394742.955
M022 (3)	6483299.574	8091228.225	7410938.518
M318 (4)	6480779.448	8102873.587	7399946.962
M804 (5)	6457066.421	8114804.583	7408133.90
THEN (6)	6476193.564	8102343.905	7404607.09
TMIC (7)	6469931.181	8105758.125	7406507.349
M_10 (8)	6470172.740	8105937.587	7406022.349
M_20 (9)	6469955.627	8105732.987	7406497.053

Table 24. Stations WGS84 cartesian coordinates of the third epoch of the real GNSS observations

# Point	X (m)	Y (m)	Z (m)
DA01 (1)	6460932.675	8105310.413	7415569.323
M020 (2)	6474138.006	8112843.571	7394742.955
M022 (3)	6483299.574	8091228.225	7410938.518
M318 (4)	6480779.448	8102873.587	7399946.962
M804 (5)	6457066.421	8114804.583	7408133.9
THEN (6)	6476193.564	8102343.905	7404607.09
TMIC (7)	6469931.181	8105758.125	7406507.349
M_10 (8)	6470172.756	8105937.214	7406022.363
M_20 (9)	6469955.62	8105733.05	7406497.541

Table 25. Stations WGS84 cartesian coordinates of the fourth epoch of the real GNSS observations

# Point	X (m)	Y (m)	Z (m)
DA01 (1)	6460932.678	8105310.412	7415569.322
M020 (2)	6474138.008	8112843.57	7394742.955
M022 (3)	6483299.576	8091228.224	7410938.517
M318 (4)	6480779.45	8102873.586	7399946.961
M804 (5)	6457066.423	8114804.582	7408133.899
THEN (6)	6476193.567	8102343.904	7404607.089
TMIC (7)	6469931.183	8105758.124	7406507.348
M_10 (8)	6470172.73	8105937.686	7406022.318
M_20 (9)	6469955.70	8105733.319	7406496.909

In the network analysis, the datum needs to be defined. This is done using an inner-constraint approach again with the contribution of all network points. After the global congruency testing, the localization step is conducted using the SATE and M-split. Moreover, the MSS using distance-difference cannot be applied either due to a change in scale existing between epochs (Ebeling (2014)).

- **Results of network analyses**

First, the observations were evaluated by the Inner-constraint approach and accepted in the second-factor variance test with a confidence level of 0.99. Second, a GCT test is performed on the displacement vector of the two-time epochs to check for the presence of displacements between the epochs in the first case.

- **Localization**

With the outcome of the GCT in mind, the next step is now to identify stable and unstable points. This is done with SATE and M-split methods. The detected stable and unstable points of each method are presented in Table (28). A Summary of the cases and methods is given in Table (32).

- **Determination of point deformation**

After the identification of all unstable and stable points, the final task is now to determine the deformations and their standard deviations. Deformations include crustal movements between the time intervals of the two mentioned epochs. (Ebeling (2014)). The network analysis is repeated, combining the observations of both epochs.

Scenario B shows that the 3D Helmert transformation can successfully on observations to get better results. The advantage of the transformation-based approach for the determination of deformations is that the adjusted coordinates and their singular cofactor matrices can directly be utilized. Furthermore, it can be applied in scenarios where different coordinate systems use.

While the MSS distance difference, is the most efficient among other methods, it cannot be used because of the scale change between two epochs (Ebeling (2014)). As we compare the two scenarios, the RMS error is lower in the transformation-based approach.

Table 26. Transformation parameters relating to local and global systems

Transformation parameter	Epoch 1-2	Epoch 1-3	Epoch 1-4
ω (rad)	-4.84e-11	-4.83e-11	-2.26e-11
φ (rad)	-1.95e-11	-1.95e-11	2.48e-10
κ (rad)	5.12e-11	5.12e-11	-2.27e-10
T_x (m)	3235691.1090	3235691.1090	3235691.1090
T_y (m)	4052599.7877	4052599.7877	4052599.7878
T_z (m)	3702940.7068	3702940.7068	3702940.7068
$(\lambda - 1) \times 10^6$	0.999	0.999	1. 0000159

Table 27. The GCT test to confirm the displacement between two epochs

T_G (Epoch 1-2)	T_G (Epoch 1-3)	T_G (Epoch 1-4)	Fisher (α=0.025, β=80)	Comment
6.73	2.71	1.99	1.616	There is possible displacement between two epochs

Table 28. The stable/unstable points using the chosen method (Fisher-distribution with α=0.025 and β=80)

	Epoch 1-2		Epoch 1-3		Epoch 1-4	
Method	M-split	SATE	M-split	SATE	M-split	SATE
Stable	1,2,3,4,5,6,7,9	1,2,3,4,5,6,7,9	1,2,3,4,5,6,7	1,2,3,4,5,6,7	1,2,3,4,5,6,7	1,2,3,4,5,6,7
Unstable	8	8	8,9	8,9	8,9	8,9

Table 29. Estimated deformations of network points in scenario B in meters

Epoch 1-2					
# Point	ΔX	ΔY	ΔZ	Norm	Direction (rad)
8	0.154	0.325	-0.552	0.659	1.128

Table 30. Estimated deformations of network points in scenario B in meters

Epoch 1-3					
# Point	ΔX	ΔY	ΔZ	Norm	Direction (rad)
8	0.171	-0.048	-0.537	0.566	-0.273
9	-0.007	0.063	0.488	0.492	1.676

Table 31. Estimated deformations of network points in scenario B in meters

Epoch 1-4					
# Point	ΔX	ΔY	ΔZ	Norm	Direction (rad)
8	0.143	0.426	-0.582	0.735	1.246
9	0.073	0.333	-0.144	0.370	1.355

Table 32. Summary of statistics for combined re-adjustment of epochs

Statics	First epoch	Second epoch
Number of points in the network	9	9
Number of observations	87	87
Number of unknowns	27	27
Redundancy	63	63
A posteriori standard deviation $\hat{\sigma}_0$	0.78	0.76
Lower boundary value $\chi^2_{S=0.025,r}$ in second-factor variance test	39.86	39.86
T_F in second-factor variance test	50.16	77.25
Upper boundary value $\chi^2_{S=0.975,r}$ in second-factor variance test	92.01	92.01
The outcome of the second-factor variance test	pass	pass
RMSE	2.04e-10	2.05e-10

3. Summary and conclusion

Deformation monitoring results are directly relevant to safety and human life. This process has an important role in carefully assessing the data to avoid wrong interpretation of the displacements (Setan and Singh (2001)). As a result, the need for a network analysis arises to combine the several types of observation and methods in the geodetic network independent of choosing an instrument (Ebeling (2014)).

In the localization step, the single-point analysis, robust estimation, and combinatorial search methods are operated. As a result of the investigation of the simulated data, the SATE and MSS using distance difference are determined as the best methods. These optimal methods are operated on the satellite real data. In general, the reason for the failure of some methods in detecting unstable points in the geodetic network, and final findings from this thesis can be stated as follows:

1. Changing the confidence interval affects the success rate. Two different cases should be recognized. First, the values of α are changed with the constant values of β. As (1- β) can show the power of each test in evaluation, the methods cannot compare equally. Second, the values of α are unchanged, with the changing values of β. By comparison of these cases, the values α=0.01, and β=20, get the best results.
2. Increasing the number of unstable points in the network reduces the success rate of methods that be affected by the geometry of the network.
3. Reducing the amount of displacement, especially in methods that use displacement vectors in their calculations, causes errors in calculations and failure to detect all unstable points in the network.
4. The existence of systematic errors in observations can cause errors in calculations. At this time, robust estimation techniques should be used, which are partially resistant to observational errors.

3. References

Acar, M., et al., 2006, Deformation analysis with total least squares: Natural Hazards and Earth System Science, **6**(4): 663-669.

Amiri-Simkooei, A., 2013, On the nature of GPS draconic year periodic pattern in multivariate position time series: Journal of Geophysical Research: Solid Earth, **118**(5): 2500-2511.

Amiri-Simkooei, A., 2018, On the use of two L1 norm minimization methods in geodetic networks: Earth Observation and Geomatics Engineering, **2**(1): 1-8.

Amiri-Simkooei, A. and J. Asgari, 2012, Harmonic analysis of total electron

contents time series: methodology and results: GPS Solutions, **16**(1): 77-88.

Amiri-Simkooei, A. R., et al. (2007). "Assessment of noise in GPS coordinate time series: methodology and results." Journal of Geophysical Research: Solid Earth 112 (B7).

Amiri-Simkooei, A., et al., 2014, Extracting tidal frequencies using multivariate harmonic analysis of sea level height time series: Journal of geodesy, **88**(10): 975-988.

Amiri-Simkooei, A., et al., 2016, Stability analysis of deformation-monitoring network points using simultaneous observation adjustment of two epochs: Journal of Surveying Engineering, **143**(1): 04016020.

Aydin, C., 2017, Effects of displaced reference points on deformation analysis: Journal of Surveying Engineering, **143**(3): 04017001.

Baarda, W., 1968, A TESTING PROCEDIJRE FOR USE IN GE, ODETIC NETWORKS.

Banaś, M., 2017, Application of Robust Estimation Methods to Displacements Determination in Geodetic Control Network of Dam. Geodetic Congress (BGC Geomatics), 2017 Baltic, IEEE.

Barbu, T. 2013, Variational image denoising approach with diffusion porous media flow. Abstract and Applied Analysis, Hindawi.

Baselga, S., et al. 2015, Deformation monitoring and the maximum number of stable points method: Measurement 70: 27-35.

Caspary, W., 1996, Anmerkungen zum robusten Schätzen: Allgemeine Vermessungs-Nachrichten, **103**(7): 287-289.

Caspary, W., 2000, Concepts of network and deformation analysis, The University of New South Wales: Kensington, Australia.

Caspary, W. and Borutta H., 1987, Robust estimation in deformation models: Survey Review, **29**(223): 29-45.

Caspary, W., et al., 1990, Deformation analysis by statistical methods: Technometrics, **32**(1): 49-57.

Chen, Y., et al., 1990, A strategy for the analysis of the stability of reference points in deformation surveys: CISM Journal, **44**(2): 39-46.

Chen, Y.-q., 1984, ANALYSIS OF DEFORMATION SURVEYS-A GENERALIZED METHOD.

Chrzanowski, A., 1986, Geotechnical and other non-geodetic methods in deformation measurements. Proc. Deformation Measurements Workshop, Massachusetts Institute of Technology, Boston.

Curran, L. P., 2008, Global navigation satellite systems for geodetic network surveys.

Demirel, H., 1987, S Transformasyonu ve Deformasyon Analizi, Türkiye 1: Bilimsel ve Teknik Kurultayı, 593: 608.

Derek, D. and Benjamin M., 1999, Remotely sensing the Earth atmosphere using GPS: The GPS/MET data analysis: Journal of Atmospheric and Oceanic Technology, **16**(8): 989-1002.

Dunnicliff, J., 1988, Geotechnical Instrumentation for Monitoring Field Performance: Wiley, New York.

Ebeling, A., 2014, Ground-Based Deformation Monitoring, University of Calgary.

Even-Tzur, G., 2006, Datum definition and its influence on the reliability of geodetic networks: Zeitschrift für Vermessungswesen, **131**(2): 87-95.

Golub, G. H. and Van Loan C. F., 1980, An analysis of the total least squares problem: SIAM journal on numerical analysis, **17**(6): 883-893.

Grafarend, E. W., 1974, Optimization of geodetic networks: The Canadian Surveyor, **28**(5): 716-723

Gründig, L., et al., 1985, Detection and localization of geometrical movements: Journal of Surveying

Engineering, **111**(2): 118-132.
http://daminfo.wrm.ir/fa/pageviewreport/854
Junhuan, P., 2005, The asymptotic variance–covariance matrix, Baarda test and the reliability of L 1-norm estimates: Journal of geodesy: **78**(11-12): 668-682.
Liu, S.-h., et al., 2016, Numerical stress-deformation analysis of cut-off wall in clay-core rockfill dam on thick overburden: Water Science and Engineering, **9**(3): 219-226.
Mohamed, A. A., 2013, Development of Geodetic Deformation Analysis Software Based on Iterative Weighted Similarity Transformation Technique, Universiti Teknologi Malaysia.
Neitzel, F., 2004, Identifizierung konsistenter Datengruppen am Beispiel der Kongruenzuntersuchung geodätischer Netze, Verlag d. Bayer. Akademie der Wiss.
Neitzel, F., 2010, Generalization of total least-squares on example of unweighted and weighted 2D similarity transformation: Journal of geodesy, **84**(12): 751-762.
Niemeier, W., 2002, Ausgleichungsrechnung: eine Einführung für Studierende und Praktiker des Vermessungs-und Geoinformationswesens, Walter de Gruyter.
Nowel, K., 2015, Robust M-estimation in analysis of control network deformations: Classical and new method: Journal of Surveying Engineering, **141**(4): 04015002.
Nowel, K., 2016, Application of Monte Carlo method to statistical testing in deformation analysis based on robust M-estimation: Survey Review, **48**(348): 212-223.
Nowel, K., 2016, Investigating efficacy of robust M-estimation of deformation from observation differences: Survey Review, **48**(346): 21-30.
Nowel, K., (2018). "Squared M split (q) S-transformation of control network deformations: Journal of geodesy, 1-20.
Nowel, K., and Kamiński W., 2014, Robust estimation of deformation from observation differences for free control networks: Journal of geodesy, **88**(8): 749-764.
Nowel, K., 2015, Robust M-estimation in analysis of control network deformations: Classical and new method: Journal of Surveying Engineering, **141**(4): 04015002.
Papo, H., 1999, Datum Accuracy and its Dependence on Network Geometry. Quo vadis geodesia, Universität Stuttgart, Technical Reports Department of Geodesy and ….
Pesonen, H., 2007, Robust estimation techniques for GNSS positioning. Proceedings of NAV07-The Navigation Conference and Exhibition, 31.10.-1.11. 2007, London, England.
Setan, H. and Singh R., 2001, Deformation analysis of a geodetic monitoring network: GEOMATICA-OTTAWA, **55**(3): 333-346.
Taşçi, L., 2008, Dam deformation measurements with GPS: Geodezija ir kartografija, **34**(4): 116-121.
Teskey, W., 1987, Integrated Analysis of Geodetic, Geotechnical, and Physical Model Data to Describe the Actual Deformation Behaviour of Earthfill Dams Under Static Loading. (Integrierte Analyse geodätischer und geotechnischer Daten sowie physikalischer Modelldaten zur Beschreibung des Deformationsverhaltens grosser Erddämme unter statischer Belastung): Institute fur Anwendungen der geodasie im Bauwesen. Universitat Stuttgart.
Teunissen, P., 2000, Adjustment theory, Series on Mathematical geodesy and positioning, Delft University Press.
Teunissen, P., et al., 2004, Probability and Observation Theory.

Van Hees, G. S., 1982, Variance-covariance transformations of geodetic networks: Manuscripta Geodaetica, **7**(1): 1-20.

Welsch, W., 1993, A general 7-parameter transformation for the combination, comparison and accuracy control of terrestrial and satellite network observations: Manuscripta Geodaetica, **18**(5): 295-295.

Welsch, W., et al., 2000, Auswertung geodätischer Überwachungsmessungen. Grundlagen, Methoden, Modelle. Ein Band der Reihe: Möser, Müller, Schlemmer, Werner (Hrsg.): Handbuch Ingenieurgeodäsie, H, Wichmann Verlag, Heidelberg.

Wiśniewski, Z., 2009, Estimation of parameters in a split functional model of geodetic observations (M split estimation): Journal of geodesy **83**(2): 105-120.

Wiśniewski, Z. 2010, M split (q) estimation: estimation of parameters in a multi split functional model of geodetic observations: Journal of geodesy, **84**(6): 355-372.

Yavaşoğlu, H., et al., 2018, Monitoring the deformation and strain analysis on the Ataturk Dam, Turkey: Geomatics, Natural Hazards and Risk, **9**(1): 94-107.